

Multiplicity scaling in ideal and viscous hydrodynamics

Huichao Song^{1,*} and Ulrich Heinz^{1,2}

¹*Department of Physics, The Ohio State University, Columbus, OH 43210, USA*

²*CERN, Physics Department, Theory Division, CH-1211 Geneva 23, Switzerland*

(Dated: May 28, 2019)

Using numerical results from ideal and viscous relativistic hydrodynamic simulations with three different equations of state, for Au+Au and Cu+Cu collisions at different centralities and initial energy densities, we explore the dependence of the eccentricity-scaled elliptic flow, v_2/ε , and the produced entropy fraction, $\Delta S/S_0$, on the final charged hadron multiplicity density dN_{ch}/dy per unit transverse overlap area S , $(1/S)dN_{\text{ch}}/dy$. The viscous hydrodynamic simulations are performed with two different versions of the Israel-Stewart kinetic evolution equations, and in each case we investigate the dependence of the physical observables on the kinetic relaxation time. We find approximate scaling of v_2/ε and $\Delta S/S_0$ with $(1/S)dN_{\text{ch}}/dy$, with scaling functions that depend on the EOS and, in particular, on the value of the specific shear viscosity η/s . Small scaling violations are seen even in ideal hydrodynamics, caused by a breaking of the scale invariance of ideal fluid dynamics by the freeze-out condition. Viscous hydrodynamics shows somewhat larger scale-breaking effects that increase with increasing η/s and decreasing system size and initial energy density. We propose to use precision studies of these scaling violations to help constrain the shear viscosity η/s of the quark-gluon plasma created in relativistic heavy ion collisions.

PACS numbers: 25.75.-q, 12.38.Mh, 25.75.Ld, 24.10.Nz

I. INTRODUCTION

Recent numerical studies of relativistic hydrodynamics for dissipative fluids [1–4] have confirmed earlier estimates [5, 6] that the “elliptic” anisotropic collective flow observed in non-central heavy-ion collisions is very sensitive to the shear viscosity of the matter formed in such collisions. Since ideal fluid dynamics (i.e. the assumption that viscosity can be neglected) provides a phenomenologically quite successful description of much of the soft hadron data collected from Au+Au collisions at the Relativistic Heavy Ion Collider (RHIC) [7–9], this implies strong constraints on the shear viscosity to entropy ratio η/s [6, 10] and the thermalization time scale [11, 12] of the matter in the collision fireball. The conclusion is that the quark-gluon plasma (QGP) created at RHIC is a strongly coupled plasma with almost perfect liquid collective behavior [13–15] whose specific shear viscosity is lower than that of any previously known real fluid and consistent with a postulated lower bound of $\eta/s \geq \hbar/(4\pi k_B)$ derived from the study of infinitely strongly coupled conformal field theories [16, 17] using the AdS/CFT correspondence and corroborated by earlier quantum mechanical arguments based on the uncertainty relation [18].

On the other hand, heavy-ion data at RHIC, SPS and AGS also show that ideal hydrodynamics gradually breaks down at larger impact parameters, for smaller collision systems, at lower collision energies, and away from midrapidity (see [9] for a review). Much of this can be attributed to strong viscous effects in the late collision stage

after the QGP has converted to hadrons [19]. However, due to uncertainties in the initial conditions for the fireball deformation, there is some room left for a non-zero value of the QGP viscosity [19]. To study this further requires a viscous hydrodynamic approach because the tool used to describe the non-equilibrium late hadronic dynamics (a classical cascade) is not well suited for the rapidly evolving, very dense matter in the early collision stages

The motivation for the present paper is provided by the well-known systematic comparison of Voloshin *et al.* [20, 21] of elliptic flow data with ideal fluid dynamical predictions which suggests that the elliptic flow parameter v_2 scaled by the initial source eccentricity ε , v_2/ε , while strongly deviating from ideal hydrodynamics at low multiplicities, still scales with the final multiplicity per unit overlap area:

$$\frac{v_2}{\varepsilon} \propto \frac{1}{S} \frac{dN_{\text{ch}}}{dy}. \quad (1)$$

For ideal fluids the right hand side is a direct measure of the initial entropy density [22]. The scaling (1) implies that all dependence on impact parameter, collision energy and system size can be, to good approximation, absorbed by simply taking into account how these control parameters change the final hadron multiplicity density. We will call this observation simply “multiplicity scaling of the elliptic flow”, where “elliptic flow” is a shorthand for the eccentricity-scaled elliptic flow v_2/ε and “multiplicity” stands for $(1/S)dN_{\text{ch}}/dy$.

Such a scaling is expected for ideal fluid dynamics whose equations of motion are scale invariant and where the eccentricity-scaled elliptic flow is therefore predicted [23, 24] to depend only on the squared speed of sound, $c_s^2 = \frac{\partial p}{\partial e}$, which describes the stiffness of the equation

*Correspond to song@mps.ohio-state.edu

of state (EOS) or “pushing power” of the hydrodynamically expanding matter. It has been known, however, for many years [25] that this ideal-fluid scaling is broken by the final freeze-out of the matter: if hadron freeze-out is controlled by hadronic cross sections (mean free paths) or simply parametrized by a critical decoupling energy density e_{dec} or temperature T_{dec} , this introduces an additional scale into the problem which is independent of (or at least not directly related to) the initial geometry of the fireball. This breaks the above argument based on scale invariance of the ideal fluid equations of motion. We will show here that this also leads to a breaking of the multiplicity scaling of v_2/ε not only in the most peripheral or lowest energy collisions, where freeze-out obviously cuts the hydrodynamic evolution short since the freeze-out density is reached before the flow anisotropy can fully build up [25], but even in the most central collisions at RHIC where freeze-out still terminates the hydrodynamic evolution before the elliptic flow can fully saturate (see also [19]).

The more interesting aspect of the experimentally observed scaling is, however, its apparent validity in regions where ideal fluid dynamics does not work (these encompass most of the available data [20]). Many years ago, simple scaling laws for the centrality dependence of elliptic flow were derived from kinetic theory in the dilute gas limit, where the particles in the medium suffer at most one rescattering before decoupling [26, 27]; these can be reinterpreted in terms of multiplicity scaling for v_2/ε . The dilute gas limit is expected to hold for very small collision systems, very large impact parameters or very low collision energies. More recently, a successful attempt was made to phenomenologically connect the dilute gas and hydrodynamic limits with a 1-parameter fit involving the Knudsen number [28]. This fit works very well for Au+Au and Cu+Cu data from RHIC, but predicts that even in the most central Au+Au collisions at RHIC the ideal fluid dynamical limit has not yet been reached and is missed by at least 25% [28]. In the present paper we use viscous relativistic hydrodynamics to explore the multiplicity scaling of v_2/ε in the phenomenologically relevant region. We conclude (not surprisingly since much of the available data is from regions where the viscous hadronic phase plays a large role [19]) that the multiplicity scaling data [20, 21] require significant shear viscosity for the medium, but also that viscous hydrodynamics predicts subtle scaling violations which seem to be qualitatively consistent with trends seen in the data (even if the experimental evidence for scaling violations is presently not statistically robust) and whose magnitude is sensitive to the specific shear viscosity η/s . This gives hope that future more precise data can help constrain the QGP shear viscosity through exactly such scaling violations.

We should caution the reader that, similar to Ref. [28] which used a constant (time-independent) Knudsen number, our viscous hydrodynamic calculations are done with a constant (temperature-independent) specific shear viscosity η/s . Neither assumption is realistic, and we expect

η/s in particular to show strong temperature dependence near T_c (the critical temperature for the quark-hadron phase transition) and emerge from the phase transition with much larger values than in the QGP phase. Comparisons between the results presented here and experimental data are therefore, at best, indicative of qualitative trends, and improved calculations, which in particular match viscous hydrodynamics to a realistic hadron cascade below T_c , are required before an extraction of η/s from experimental data can be attempted.

II. DISSIPATIVE FLUID DYNAMICS

In this section we briefly review the viscous hydrodynamic equations that we solve, focussing on some differences in the formulations used in previously published papers [1–4] which we investigate here further. For technical details we ask the reader to consult these earlier papers.

We focus on systems with exact longitudinal boost-invariance and use the code VISH2+1 [3] to solve numerically for the expansion in the two dimensions transverse to the beam direction. As in [1–4] we consider only shear viscosity, neglecting bulk viscosity and heat conduction. (Bulk viscosity may become large near the QCD phase transition [29–31] and should thus be included in the future before comparing viscous hydrodynamics with experimental data.) VISH2+1 solves the conservation laws for energy and momentum, $d_m T^{mn} = 0$ (where d_m is the covariant derivative in our curvilinear (τ, x, y, η) coordinate system [32]), with the decomposition

$$T^{mn} = eu^m u^n - p\Delta^{mn} + \pi^{mn}, \quad \Delta^{mn} = g^{mn} - u^m u^n, \quad (2)$$

together with evolution equations for the viscous shear pressure tensor components π^{mn} :

$$D\pi^{mn} = -\frac{1}{\tau_\pi}(\pi^{mn} - 2\eta\sigma^{mn}) - (u^m \pi^{nk} + u^n \pi^{mk})Du_k - \frac{1}{2}\pi^{mn}\frac{\eta T}{\tau_\pi}d_k\left(\frac{\tau_\pi}{\eta T}u^k\right) - \pi_a^{(m}\omega^{n)a}. \quad (3)$$

Here $D = u^m d_m$ is the time derivative in the local co-moving frame, $\nabla^m = \Delta^{ml}d_l$ is the spatial gradient in that frame, and $\sigma^{mn} = \nabla^{(m}u^{n)} = \frac{1}{2}(\nabla^m u^n + \nabla^n u^m) - \frac{1}{3}\Delta^{mn}\theta$ (with the scalar expansion rate $\theta \equiv d_k u^k = \nabla_k u^k$) is the symmetric and traceless velocity shear tensor. $\omega_{mn} = \nabla_n u_m - \nabla_m u_n$ is the vorticity tensor, and $a^{(m}b^{n)} \equiv \frac{1}{2}(a^m b^n + a^n b^m)$ denotes symmetrization. Even though several components of the symmetric shear pressure tensor π^{mn} are redundant [32] on account of its tracelessness and transversality to the flow velocity u^m , VISH2+1 propagates all 7 non-zero components and uses the tracelessness and transversality conditions as checks of the numerical accuracy [3].

For a conformally symmetric fluid such as a massless quark-gluon gas, the temperature T is the only scale in the problem and therefore $\eta \sim s \sim T^3$ and $\tau_\pi \sim 1/T$,

hence $\eta T/\tau_\pi \sim T^5$. In this limit the first term in the second line of Eq. (3) can be written as [33]

$$-\frac{1}{2}\pi^{mn}\frac{\eta T}{\tau_\pi}d_k\left(\frac{\tau_\pi}{\eta T}u^k\right)=+\frac{1}{2}\pi^{mn}(5D(\ln T)-\theta). \quad (4)$$

This is the form used in Ref. [1].

It has recently been argued [34–37] that the r.h.s. of Eq. (3) should contain even more terms, at least for conformal fluids in the strong coupling limit. We will not pursue this possibility here.

Equations (3) are known as “Israel-Stewart (I-S) equations” and based on an expansion of the entropy production rate to second order [33, 38–41] (macroscopic approach) or, in a microscopic kinetic approach using Grad’s 14-moment method, of the phase-space distribution function to first order in small deviations from local thermal equilibrium [38, 41, 42] (see also [43]). By introducing a finite and sufficiently large relaxation time τ_π for the evolution of the shear pressure tensor towards its Navier-Stokes limit $\pi^{mn} = 2\eta\sigma^{mn}$, these equations eliminate problems with acausal signal propagation at short wavelengths and the resulting numerical instabilities that famously plague the relativistic Navier-Stokes equation. A somewhat different approach to solving these problems was developed by Öttinger and Grmela (Ö-G) [44] and has been used in [4]; because a comparison of results obtained with the I-S and Ö-G equations is non-trivial, we will leave that for a later study.

Refs. [1–3] use different versions of Eqs. (3). P. & U. Romatschke [1] use the full set of terms displayed in (3) which we label as “full I-S equation”. The last term in the second line of Eq. (3) involving the vorticity cannot be obtained from the macroscopic approach [32, 40] since it does not contribute to entropy production, but it follows from the microscopic kinetic approach [38, 42]. For longitudinally boost-invariant systems with initially vanishing transverse flow it is zero initially and was found in [1] to remain tiny throughout the fireball evolution. We can therefore remove it from consideration when comparing published results from the different approaches. The first term in the second line of (3) arises in this form from the macroscopic approach (2nd order entropy production [32, 40]) but was neglected in our previous work [3], following an argument in [32] that it is of second order in small quantities and therefore subdominant compared to the first two terms on the r.h.s. of Eq. (3). A similar argument can be made for the last term in line 1 of (3) (which does not contribute to entropy production either), but Baier *et al.* [42] pointed out that this term is needed to preserve the transversality of π^{mn} during kinetic evolution. In Ref. [3] we therefore kept all terms in the *first* line of Eq. (3) but dropped those in the *second* line; we call this here the “simplified I-S equation”. In Ref. [34] Baier *et al.* argued that for a conformally invariant medium, such as a classical massless quark-gluon gas, the first term in the *second* line is needed to preserve the conformal invariance of the kinetic evolution equation and hence should not be dropped. We now understand

that the arguments presented in [32] to neglect all but the first term on the right hand side of Eq. (3) were at best superficial since this term involves the difference between two first-order quantities and thus presumably needs to be counted as small of second order.

Chaudhuri followed in his work [2] the approach advertised in [32]; as a result, in his procedure π^{mn} must be expected to evolve away from transversality. He circumvents this problem by evolving only the three linearly independent components of π^{mn} and computing the rest from the tracelessness and transversality conditions [2]. The problem resurfaces, however, since now the results for all components of π^{mn} must be expected to depend on the choice of independent components which are evolved dynamically with the truncated equation (3). While these questions await quantitative study we note that Chaudhuri’s results [2] appear to differ significantly from ours [3].

In the present paper we show many comparisons between solutions obtained by using the “full I-S equations” with those from the “simplified I-S equations”. Although at sufficiently long wavelengths both have to agree in the Navier-Stokes limit $\tau_\pi \rightarrow 0$ (up to issues of numerical stability), as inspection of Eq. (3) readily shows, they differ for non-zero τ_π and will be seen to exhibit different degrees of sensitivity to τ_π . This is of phenomenological importance since τ_π for the QGP is not known, and a strong sensitivity to this unknown parameter will negatively impact our ability to extract the QGP shear viscosity η/s from experimental data.

III. INITIAL CONDITIONS, FREEZE-OUT, AND EQUATION OF STATE

For the present study, we initialize the expanding fireball in the same way as in Ref. [3], i.e. with vanishing initial transverse flow and with an initial energy density profile proportional to the transverse density of wounded nucleons, calculated from a Saxon-Woods nuclear density profile with radius and surface thickness parameters $R_0 = 4.2$ fm, $\xi = 0.596$ fm for Cu and $R_0 = 6.37$ fm, $\xi = 0.56$ fm for Au nuclei. The energy density profile is normalized by a parameter $e_0 = e(\tau_0; r=b=0)$ giving the peak energy density in the center of the fireball for central collisions (impact parameter $b = 0$). e_0 is related to the peak wounded nucleon density in the same collisions by a factor κ which is assumed to depend on energy but not on the size of the colliding nuclei. We here consider e_0 values that lead to final multiplicities covering the range accessible at RHIC and beyond, albeit perhaps not all the way to the Large Hadron Collider (LHC).

As of now, the energy dependence of κ cannot be calculated and must be determined empirically from the final charged hadron multiplicity dN_{ch}/dy . Since dN_{ch}/dy counts the final entropy per unit of rapidity, including any entropy generated by viscous effects during the expansion, the value of dN_{ch}/dy corresponding to a given

κ will depend on the viscosity η/s . We will see that the amount of entropy produced by viscous effects additionally depends on system size, impact parameter and collision energy, but that all these dependences can, to good approximation, be absorbed in a single scaling function, with parametric dependence on η/s , that depends only on the multiplicity density $(1/S)dN_{\text{ch}}/dy$: similar to v_2/ε , entropy production $\Delta S/S_0$ exhibits approximate “multiplicity scaling”. However, this scaling function turns out to be non-linear. It therefore modifies the centrality dependence of the produced charged multiplicity, softening the observed increase with collision centrality of the produced charged multiplicity per pair of wounded nucleons, $2\frac{dN_{\text{ch}}/dy}{N_{\text{part}}}$. Exploration of this important issue requires an accurate modeling of the impact parameter dependence of the initial entropy density profile using, say, the Glauber or color glass condensate models. This is beyond the scope of the present article and will be left for a future study.

Following the majority of previous studies [2–4, 45, 46], the viscous shear pressure tensor is initialized with its Navier-Stokes value $\pi^{mn} = 2\eta\sigma^{mn}$. Other initial conditions were studied in [1, 3], but the final observables were found to be insensitive to such variations [3]. The kinetic relaxation time τ_π for the kinetic evolution of the shear pressure tensor is taken as $\tau_\pi = c_\pi\tau_\pi^{\text{Boltz}}$ where $\tau_\pi^{\text{Boltz}} = \frac{6}{T}\frac{eta}{s}$ is the kinetic theory value for a classical gas of massless Boltzmann particles [38] and c_π is varied between $\frac{1}{4}$ and 1.

Decoupling from the hydrodynamic fluid is implemented by following the same procedure as described in [3]. We use the AZHYDRO algorithm [47] to find the freeze-out surface at constant decoupling temperature $T_{\text{dec}} = 130\text{ MeV}$ and calculate the final hadron spectra from the Cooper-Frye integral over this surface [48], with a distribution function that accounts for the remaining small deviations from local thermal equilibrium along that surface [3, 6]. Resonance decays are neglected, and only the elliptic flow of directly emitted pions is shown. To estimate the total charged hadron multiplicity, we take the directly emitted positive pions, multiply by 1.5 to roughly account for multiplication by resonance decays at T_{dec} , then multiply by another factor $2 \times 1.2 = 2.4$ to account for the negatives and roughly 20% of final charged hadrons that are not pions. A proper calculation of the resonance decay chain is computationally expensive and, for a systematic study like the one presented here that requires hundreds of runs of VISH2+1, beyond our presently available resources.

Figure 1 shows the three equations of state (EOS) explored in the present study. EOS I describes a non-interacting gas of massless particles, $e = p/3$. EOS Q is a frequently employed equation of state [25] that matches a non-interacting quark-gluon gas above T_c in a first-order transition (Maxwell construction) to a realistic hadron resonance gas (HRG) in chemical equilibrium below T_c , using a bag parameter B to adjust T_c to $T_c = 164\text{ MeV}$. SM-EOS Q is a slightly smoothed version of EOS Q, see

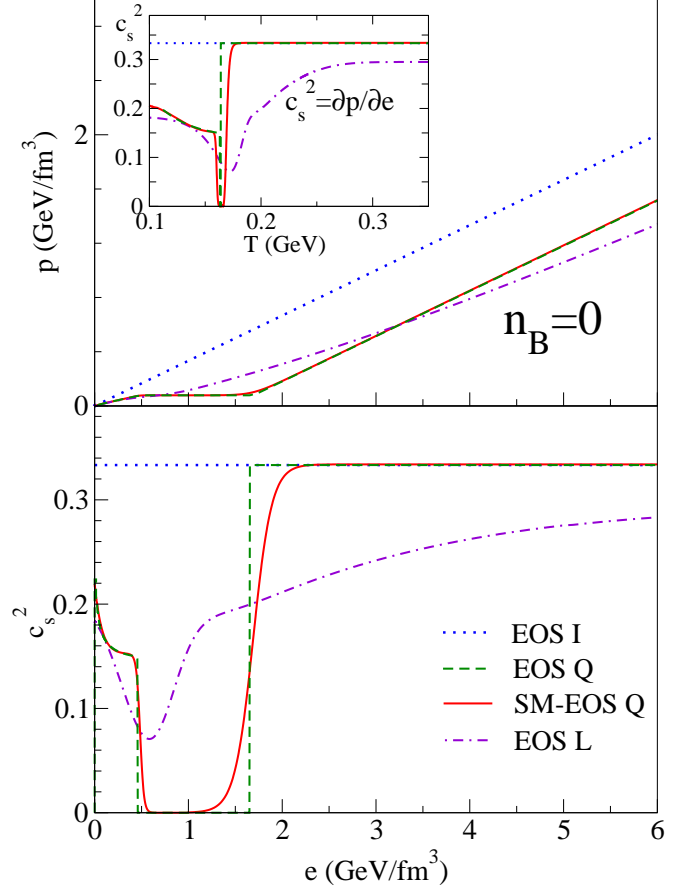


FIG. 1: (Color online) The equation of state. The upper plot shows the pressure p as a function of energy density e and (in the inset) the squared speed of sound $c_s^2 = \frac{\partial p}{\partial e}$ as a function of temperature T . The lower panel shows c_s^2 as a function of energy density e .

[3] for details. Since the discontinuities in the function $c_s^2(e)$ for EOS Q cause numerical problems in VISH2+1 due to large velocity gradients near the interfaces between QGP, mixed phase and HRG, we here use SM-EOS Q.

EOS L matches the same hadron resonance gas below T_c smoothly in a rapid cross-over transition to lattice QCD data [49] above T_c . For the fit, the lattice data were plotted in the form $p(e)$, interpolated and then smoothly joined to the $p(e)$ curve of the HRG. As can be seen in the upper panel of Fig. 1 in the inset, our procedure is not fully thermodynamically consistent and leads to a somewhat different temperature dependence of c_s^2 below T_c than for EOS Q and SM-EOS Q. Since this only affects the flow dynamics below our decoupling temperature of $T_{\text{dec}} = 130\text{ MeV}$, we have not put any effort into correcting this. For future comparisons of viscous hydrodynamic calculations with experimental data, the chemical equilibrium hadron resonance gas below T_c employed here must be replaced by a chemically non-equilibrated hadron gas whose particle ratios are frozen in

at the chemical decoupling temperature $T_{\text{chem}} \approx T_c$; this has well-known consequences for the final hadron spectra and elliptic flow which can not be neglected [50]. We postpone this, together with a more careful and thermodynamically fully consistent matching to the lattice QCD data, to a future study. We note, however, that EOS L shown in Fig. 1 is quite similar to EOS qp studied in Ref. [51].

IV. EVOLUTION OF MOMENTUM ANISOTROPIES: SIMPLIFIED VS. FULL I-S EQUATIONS

It has been previously observed that the results of Refs. [1] and [3] for the differential elliptic flow $v_2(p_T)$, although both based on the Israel-Stewart 2nd order formalism, seemed to disagree, our work [3] showing much stronger viscous suppression of v_2 than that of P. & U. Romatschke [1]. The resolution of this discrepancy was made difficult by the fact that the two groups not only used different versions of the Israel-Stewart equation (3) as described in Sec. II, but also different initial conditions, different equations of state, and system sizes (Cu+Cu [3] vs. Au+Au [1]). In [3] we noted in a footnote that the main reason for the observed differences seemed to be the different I-S equations used by the two groups. As we will see, this is only part of the story. In this sections we explore this question further and lead it to a complete resolution.

Figure 2 shows the temporal evolution of the total momentum anisotropy $\varepsilon_p = \frac{\langle T^{xx} - T^{yy} \rangle}{\langle T^{xx} + T^{yy} \rangle}$ averaged over the transverse plane¹ for two collision systems (Cu+Cu at $b = 7$ fm on the left, Au+Au at $b = 7$ fm on the right) and three equations of state (EOS I (top), SM-EOS Q (middle), and EOS L (bottom)). The blue dashed lines at the top indicate the result from ideal fluid dynamics, the black and orange lines below show viscous fluid dynamical results. The black lines show solutions of the full I-S equations, the orange ones for the simplified I-S approach; in each case several values of the kinetic relaxation time τ_π are explored. Note that our full I-S equations (3) do not use the identity (4) used in [1] which strictly holds only for conformal fluids (i.e. for the case of EOS I in Fig. 2). We have, however, tested the two expressions on the left and right of Eq. (4) against each other also for the other two equations of state (SM-

EOS Q and EOS L) which are not conformally invariant, and found no discernible differences. Only for a very long relaxation time $\tau_\pi = 12\eta/sT$ (not shown in Fig. 2) did we see for EOS L a difference larger than the line width, with our result for ε_p lying slightly above the one obtained with the conformal approximation (4).

Comparison of the black and red lines in Fig. 2 shows that the sensitivity of the momentum anisotropy ε_p to the relaxation time τ_π is significantly larger for the simplified I-S equations (red) than for the full I-S equations, and that the τ_π -dependence of ε_p even has the opposite sign for the two sets of equations. With the full I-S equations, ε_p moves slowly towards the ideal fluid limit as τ_π increases whereas with the simplified I-S equations ε_p moves away from the ideal fluid limit, at a more rapid rate, resulting in a larger viscous suppression of the momentum anisotropy. In the limit $\tau_\pi \rightarrow 0$, both formulations approach the same Navier-Stokes limit. The difference between full and simplified I-S equations is largest for EOS I which is the stiffest of the three studied equations of state, causing the most rapid expansion of the fireball. For this EOS, the simplified I-S equations allow for the largest excursions of π^{mn} away from its Navier-Stokes limit, causing a significant and strongly τ_π -dependent increase of all viscous effects, including the suppression of the momentum anisotropy (Fig. 2) and elliptic flow (see Fig. 4 below) and the amount of viscous entropy production (see Sec. VI).

For the other two equations of state, SM-EOS Q and EOS L, the difference between full and simplified I-S dynamics is much smaller, ranging from $\sim 5\%$ for Au+Au to $\sim 15\%$ for Cu+Cu for the largest τ_π value of $6\eta/sT$ studied here. Note that the viscous suppression of ε_p is much stronger for the smaller Cu+Cu collision system than for Au+Au. For SM-EOS Q and EOS L (which yield rather similar results for ε_p , with differences not exceeding $\sim 10\%$), the results from the full I-S equations (black lines) are almost completely independent of τ_π , even for the small Cu+Cu system.

The insets in the two upper panels of Fig. 2 illustrate the different τ_π -dependences for ε_p in the full and simplified I-S formulations, by plotting the value of ε_p for EOS I at a fixed time $\tau - \tau_0 = 4 \text{ fm}/c$ as a function of τ_π . One sees that, for the investigated range of relaxation times, the τ_π -dependence is linear, but that the slope has different signs for the full and simplified I-S equations and is much smaller for the full I-S system. Even though VISH2+1 cannot be run for much smaller τ_π values, due to numerical instabilities that develop as the Navier-Stokes limit $\tau_\pi = 0$ is approached, the lines corresponding to the full and the simplified I-S equations are seen to nicely extrapolate to the same Navier-Stokes point, as they should. For SM-EOS Q and EOS L, the corresponding lines may no longer be linear, due to phase transition effects, but are still characterized by opposite slopes for the simplified and full I-S approaches, with almost vanishing slope in the full I-S case. This agrees with findings reported in [1, 52].

¹ Note that ε_p as defined here includes the effects from both flow velocity and shear pressure anisotropies [3]. In Ref. [3] we denoted it by ε'_p in order to distinguish it from the flow-induced momentum anisotropy $\frac{\langle T_0^{xx} - T_0^{yy} \rangle}{\langle T_0^{xx} + T_0^{yy} \rangle}$ which is based only on the ideal fluid part of the energy momentum tensor and neglects anisotropies in the local fluid rest frame caused by the shear pressure tensor π^{mn} . In the present work we drop the prime for convenience.

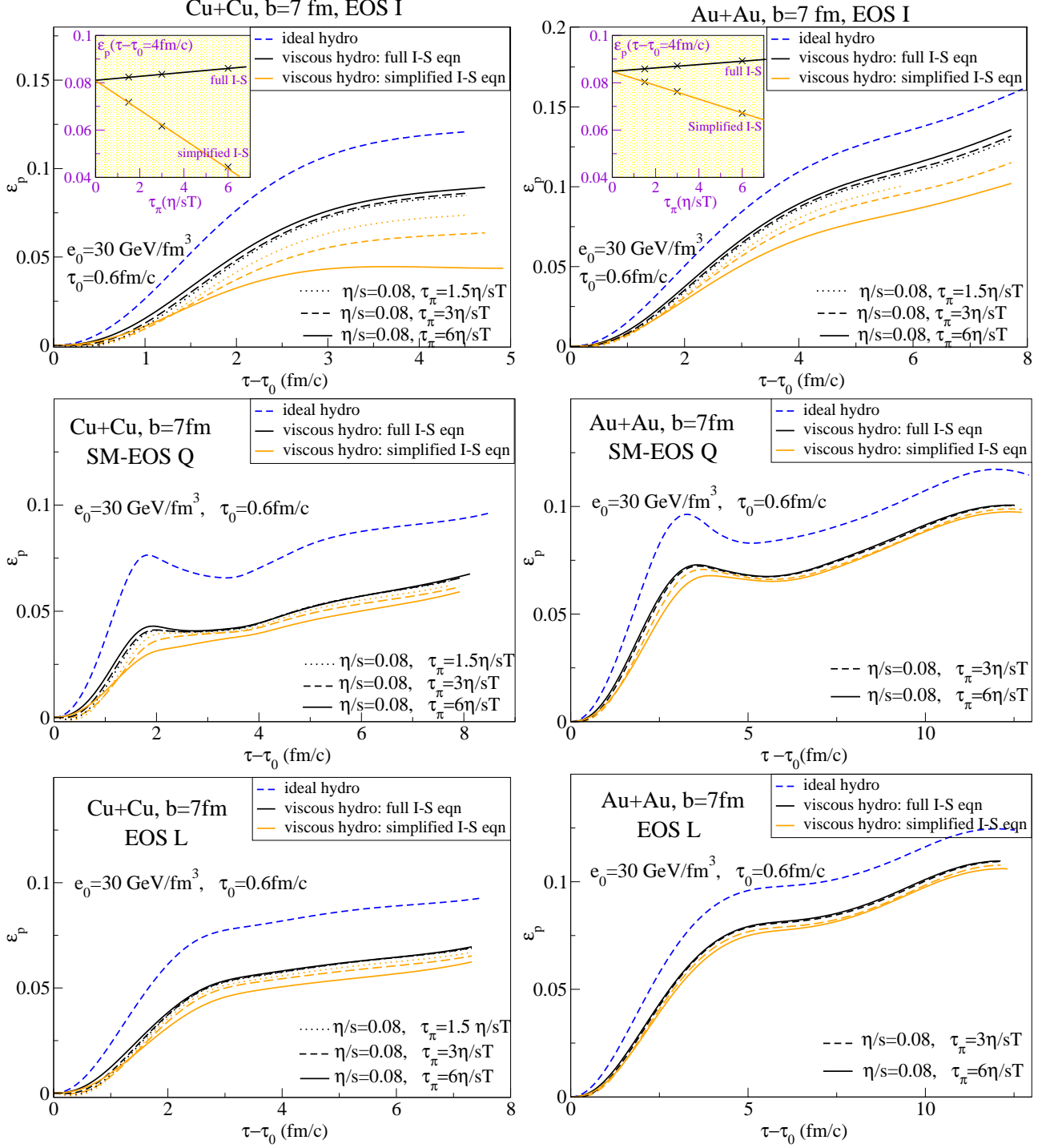


FIG. 2: (Color online) Time evolution of the total momentum anisotropy ε'_p for two collision systems (left: Cu+Cu; right: Au+Au), three equations of state (top: EOS I; middle: SM-EOS Q; bottom: EOS L), and three values of the kinetic relaxation time τ_π as indicated (dotted, dashed and solid curves, respectively). The insets in the two top panels show the τ_π -dependence of the momentum anisotropy ε_p at fixed time $\tau - \tau_0 = 4 \text{ fm/c}$. See text for discussion.

In Fig. 3 the effects of changing the system size, EOS, and form of I-S equations on the differential elliptic flow $v_2(p_T)$ for directly emitted pions is shown. The largest viscous suppression of elliptic flow (by almost 70% below the ideal fluid value at $p_T = 2 \text{ GeV/c}$) is seen for

the small Cu+Cu system, evolved with SM-EOS Q and the simplified I-S equation. This is the result reported by us in [3]. The middle panel of Fig. 3 shows that this large v_2 suppression is almost cut in half by going from Cu+Cu to Au+Au, the system studied in [1], even with-

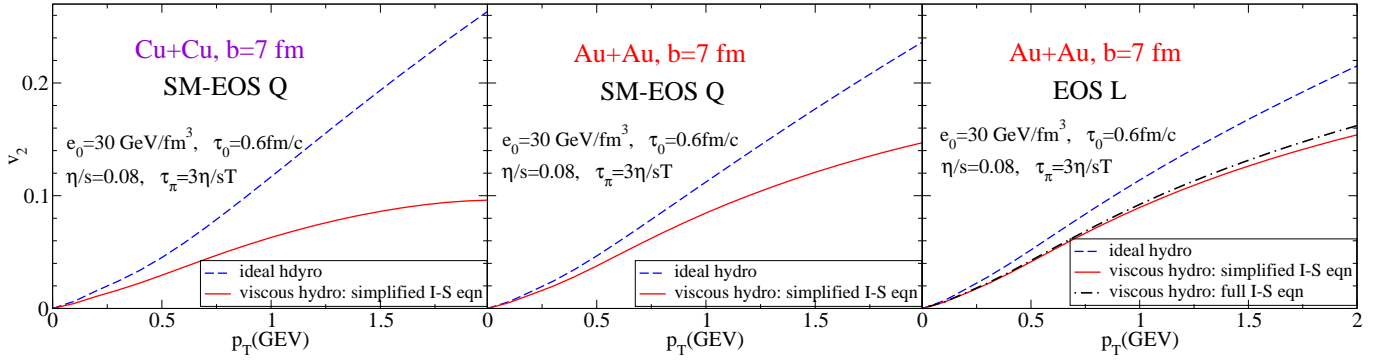


FIG. 3: (Color online) Differential elliptic flow $v_2(p_T)$ for directly emitted pions (i.e. without resonance decay contributions), comparing results for different collisions systems and equations of state. Left: Cu+Cu at $b = 7$ fm with SM-EOS Q. Middle: Au+Au at $b = 7$ fm with SM-EOS Q. Right: Au+Au at $b = 7$ fm with EOS L. Dashed (solid) lines correspond to ideal (viscous) fluid dynamics, with parameters as indicated.

out modifying the EOS or the form of the I-S equations. Changing the EOS from SM-EOS Q [3] to EOS L (which is close to the one used in [1]) reduces the viscous v_2 suppression by another quarter, from about 40% to less than 30% below the ideal fluid limit at $p_T = 2$. Finally, replacing the simplified I-S equations used in [3] by the full I-S equations employed by Romatschke [1] further reduces the suppression from about 28% below the ideal fluid to $\sim 25\%$ at $p_T = 2$ GeV/c. This is consistent with the results obtained [1].

We conclude that the biggest contribution to the large difference between the results reported in Refs. [3] and [1] arises from the different collisions systems studied, with much larger viscous effects seen in the smaller Cu+Cu system than in Au+Au collisions. The next most important sensitivity is to the EOS; for the most realistic EOS studied here, EOS L, the differences between using the full or simplified I-S equations with $\tau_\pi = 3\eta/sT$ are only about 10% on a relative scale, or about 3% on the absolute scale set by the elliptic flow from ideal fluid dynamics. For smaller τ_π , this last difference would shrink even further.

The sensitivity to details of the EOS documented by the middle and right panels of Fig. 3 gives an idea of how well one needs to know the EOS if one wants to extract the specific shear viscosity η/s from experimental data using viscous hydrodynamics. One might argue that the difference between a first order phase transition implemented through SM-EOS Q and a smooth crossover as in EOS L should be sufficiently extreme to cover the maximal theoretical uncertainty. In this case, Fig 3 tells us that the maximal theoretical uncertainty on the viscous suppression of v_2 (and therefore on η/s) should be about 25-30%. This should be compared to the theoretical error introduced by our present uncertainty of the initial spatial source eccentricity ε : ε differs by about 30% between initializations based on the Glauber and color glass condensate (CGC) models [19, 52–54], resulting in a $\sim 30\%$ uncertainty of the total magnitude of the elliptic flow in ideal fluid dynamics. We further caution that

recent discussions about the value of the critical temperature for the quark-hadron transition [55, 56] introduce an additional moment of uncertainty which is perhaps not covered by the range between SM-EOS Q and EOS L studied here. Therefore, while we agree with the authors of Ref. [52] that the uncertainty about the initial source eccentricity dominates over uncertainties related to different implementations of the I-S formalism, we think that the EOS should not be discounted prematurely as a possible source of significant additional theoretical uncertainty in the extraction of η/s .

V. MULTIPLICITY SCALING OF v_2/ε IN IDEAL AND VISCOUS HYDRODYNAMICS

In this section we explore the multiplicity scaling (as defined in the Introduction) of the eccentricity-scaled elliptic flow v_2/ε , comparing ideal fluid dynamics with that of near-minimally viscous fluids with specific shear viscosity $\frac{\eta}{s} = \mathcal{O}\left(\frac{1}{4\pi}\right)$.

A. EOS I: conformal fluids with $e = 3p$

We begin with the simple case of a conformal fluid with the equation of state $e = 3p$ (EOS I), without phase transition. In this case the speed of sound is a constant, independent of temperature T , $c_s^2 = \frac{1}{3}$. For the ideal fluid case, naive scaling arguments based on the scale invariance of the ideal fluid equations of motion would thus predict a constant v_2/ε , independent of multiplicity density $(1/S)dN_{ch}/dy$. (The nuclear overlap area S is computed as $S = \pi\sqrt{\langle x^2 \rangle \langle y^2 \rangle}$ where $\langle \dots \rangle$ denotes the energy density weighted average over the transverse plane.) The left panel in Fig. 4 clearly contradicts this expectation. Freeze-out at $T_{dec} = 130$ MeV cuts the hydrodynamic evolution of the momentum anisotropy ε_p short before the elliptic flow has fully saturated. As the left panel of the figure shows, this not only causes a strong suppres-

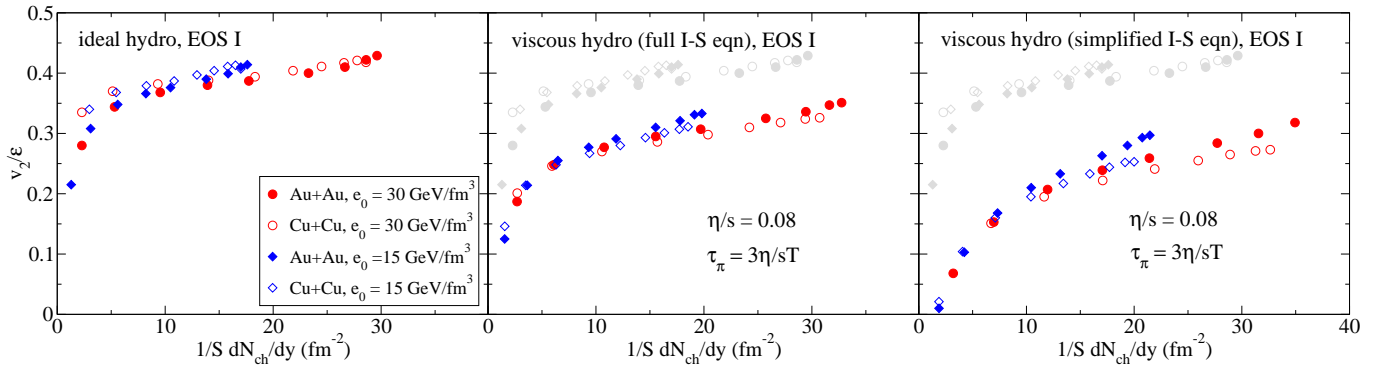


FIG. 4: (Color online) The eccentricity-scaled elliptic flow v_2/ε as a function of charged multiplicity density, $(1/S)dN_{ch}/dy$, for a conformal fluid with EOS I. Results for Cu+Cu and Au+Au collisions with two different initial energy densities at a variety of impact parameters, as indicated in the legend, are superimposed. Results from ideal fluid dynamics (left panel) are compared with those from viscous hydrodynamics, using the full (middle panel) and the simplified (right panel) Israel-Stewart equations, respectively. In all cases approximate, but not perfect multiplicity scaling is observed (see text for discussion). In the middle and right panel, the ideal fluid results from the left panel are reproduced as gray symbols for comparison.

sion of v_2/ε at low multiplicity densities, where the time between beginning of the hydrodynamic expansion and freeze-out becomes very short, but it also breaks the multiplicity scaling at high multiplicity density, albeit more weakly. At a fixed value of $(1/S)dN_{ch}/dy$, one sees larger v_2/ε for more central collisions initiated at lower collision energies (corresponding to smaller e_0 parameters) than for more peripheral collisions between the same nuclei at higher beam energies, and also for more central Cu+Cu collisions (with a rounder shape) than for more peripheral Au+Au collisions (with a more deformed initial shape). We find that the larger v_2/ε values can be traced directly to somewhat longer lifetimes of the corresponding fireballs, i.e. to the availability of more time to approach the saturation values of the momentum anisotropy and elliptic flow before reaching freeze-out. These freeze-out induced scaling violations in ideal fluid dynamics disappear at sufficiently high collision energies (i.e. large e_0) where the momentum anisotropy has time to fully saturate in *all* collision systems and at *all* impact parameters, before freezing out.

The middle and right panels in Fig. 4 show the analogous results for a minimally viscous fluid with $\frac{\eta}{s} = \frac{1}{4\pi}$ and kinetic relaxation time $\tau_\pi = \frac{3\eta}{sT}$. Consistent with the discussion in the preceding section, the viscous suppression of the elliptic flow is seen to be stronger if the simplified I-S equations are used (right panel) than for the full I-S equation. (Although not shown, the curves in the right panel also show stronger sensitivity to the value of τ_π than those in the middle panel.) Along with the suppression of v_2/ε by shear viscosity we see the appearance of scale-breaking effects that increase in proportion to the overall suppression of elliptic flow: they are larger in the right than in the middle panel. Shear viscosity breaks the multiplicity scaling of v_2/ε because (as shown in the preceding section) viscous effects are larger in smaller collision fireballs. Consequently, if we compare different collision systems that produce the same charged

multiplicity density $(1/S)dN_{ch}/dy$, we find smaller v_2/ε for Cu+Cu than for Au+Au collisions, and for peripheral Au+Au collisions at higher collision energy than for more central Au+Au collisions at lower collision energy.

Viscous effects also generate entropy, i.e. they increase the final charged multiplicity dN_{ch}/dy . Comparing in the middle and right panels of Fig. 4 the gray (shaded) symbols from ideal fluid dynamics with the colored (solid) symbols for viscous hydrodynamics, points corresponding to the same collision system and impact parameter are seen to be shifted to the right. This enhances the scaling violations: for a given collision system, impact parameter and collision energy, viscosity decreases the eccentricity scaled elliptic flow v_2/ε , pushing the corresponding point downward in the diagram, and simultaneously increases the entropy, pushing the corresponding point horizontally to the right. The combination of these two effects separates the curves for different collision systems and energies farther in viscous hydrodynamics than in ideal fluid dynamics.

B. Phase transition effects: EOS Q and EOS L

Figure 5 shows the analogous results if the fluid evolves under the influence of an equation of state with a quark-hadron phase transition, EOS Q (top row) or EOS L (bottom row). Again approximate multiplicity scaling of v_2/ε is observed, but small scale-breaking effects are visible in both ideal and viscous hydrodynamics. For the equations of state with a phase transition, the scale-breaking effects are actually larger in the ideal than in the viscous case, i.e. *in viscous hydrodynamics v_2/ε shows better multiplicity scaling than in ideal fluid dynamics!* We interpret the large scale-breaking effects in the ideal fluid case as a complication arising from interference between the freeze-out process and the weak acceleration of matter in the phase transition region. This interpretation

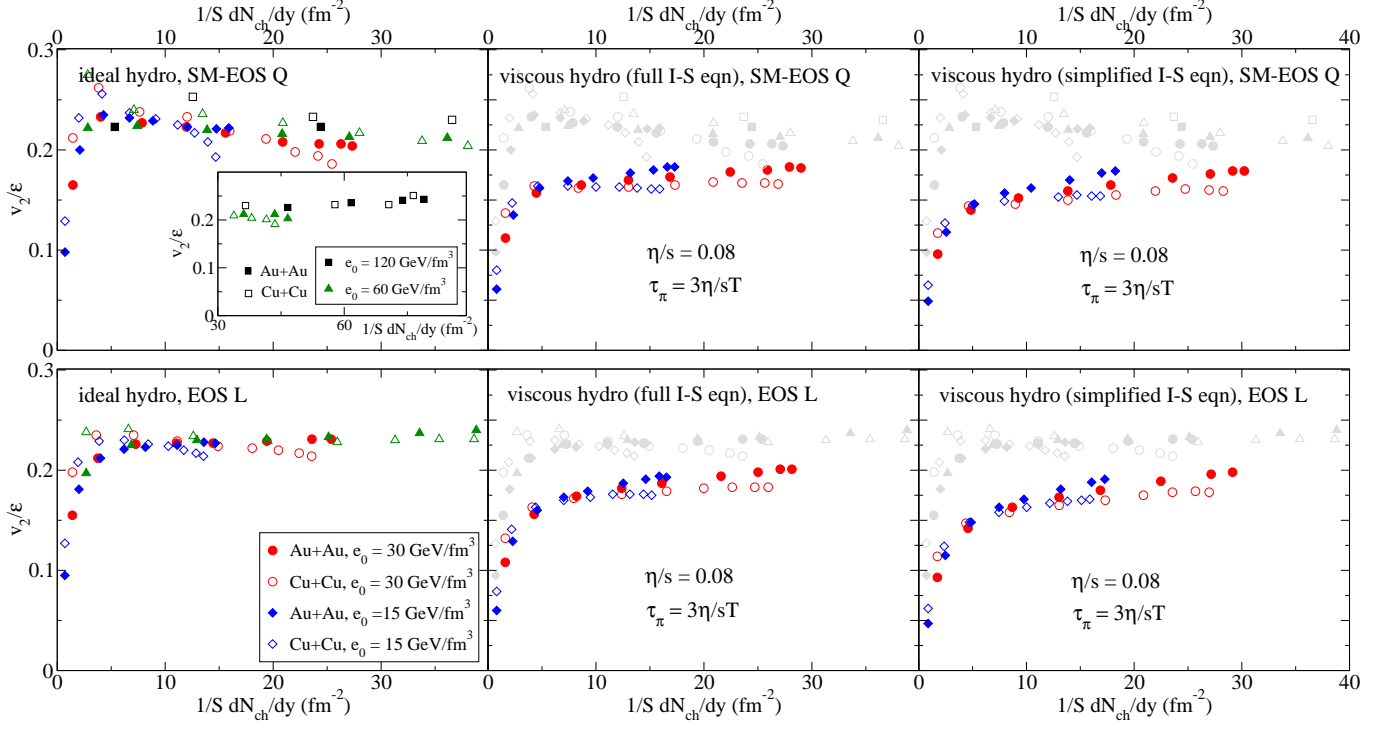


FIG. 5: (Color online) Same as Fig. 4, but for SM-EOS Q (top row) and EOS L (bottom row). For the ideal fluid case (left panels), an extended range of e_0 values up to $e_0 = 120$ GeV/fm³ was studied, in order to show that v_2/ϵ eventually increases again at higher collision energies [25].

is supported by a comparison between SM-EOS Q with its first-order phase transition (upper left panel in Fig. 5) and the smooth crossover transition in EOS L (lower left panel): for ideal fluids, the scale-breaking effects are obviously larger for SM-EOS Q than for EOS L. As already observed in [3], shear viscosity effectively smears out the phase transition and reduces its effect on the dynamics. In Fig. 5 this is clearly seen on the left side of each panel (i.e. at small values of $\frac{1}{S} \frac{dN_{ch}}{dy}$) where for the ideal fluid v_2/ϵ shows a non-monotonic peak structure [25] that is completely gone in the viscous case.

Comparing Figs. 4 and 5, we see much smaller differences between the full (middle panels) and simplified I-S equations (right panels) for SM-EOS Q and EOS L than for EOS I. This is consistent with our observations in Sec. IV where the largest differences between full and simplified I-S equations was also seen for the rapidly evolving fireballs whose expansion is pushed by the very stiff EOS I.

It is interesting to observe that, for ideal fluids, EOS L leads to about 10% more elliptic flow under RHIC conditions than SM-EOS Q. The reason is that in the phase transition region EOS L is stiffer than SM-EOS Q. This plays an important role at RHIC because the softness of the EOS near T_c inhibits the buildup of elliptic flow exactly under RHIC conditions [25]. As a corollary we note that, if RHIC elliptic flow data exhaust ideal fluid predictions made with SM-EOS Q [8], they will not exhaust

ideal fluid predictions based on EOS L, thus leaving some room for shear viscous effects.

C. Viscous suppression of v_2 : systematics

Even at the highest collision energies (or e_0 values) studied in Figs. 4 and 5, the slope of v_2/ϵ as a function of $\frac{1}{S} \frac{dN_{ch}}{dy}$ remains positive, i.e. v_2/ϵ continues to increase and evolve in direction of the asymptotic ideal fluid limit. This implies that at higher collision energies the importance of viscous effects decreases. This observation parallels the one made in [3], namely that with increasing collision energy the p_T range increases over which viscous hydrodynamic predictions for the single-particle momentum spectra can be trusted. The reason is in both cases that with increasing collision energy the time until freeze-out grows, and that (at least for constant η/s as assumed here and in [3]) during the later stages of the expansion shear viscous effects are small.

Figure 6 shows this more quantitatively. We plot the fractional decrease of the elliptic flow relative to its ideal fluid dynamical value, $(v_2^{\text{ideal}} - v_2^{\text{viscous}})/v_2^{\text{ideal}}$, as a function of multiplicity density. Larger multiplicity densities lead to smaller viscous suppression effects. Larger viscosity results in stronger suppression of the elliptic flow. The suppression effects are weaker if the full I-S equations are used than in the simplified approach of Ref. [3]

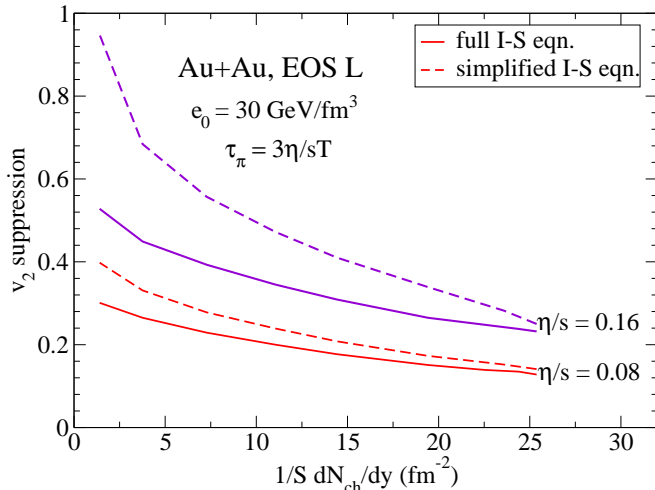


FIG. 6: (Color online) Viscous suppression of elliptic flow, $(v_2^{\text{ideal}} - v_2^{\text{viscous}})/v_2^{\text{ideal}}$, as a function of $(1/S)dN_{\text{ch}}/dy$ for Au+Au with EOS L, $\tau_\pi = 3\eta/sT$ and two values of η/s as indicated. Solid (dashed) lines correspond to using the full (simplified) I-S equations, respectively.

(which, as discussed in Sec. IV, also suffers from strong sensitivity to τ_π). For minimal viscosity, $\eta/s = 1/4\pi$, the p_T -integrated elliptic flow v_2 in Au+Au collisions at RHIC is suppressed by about 20%. The suppression is larger at lower energies but will be less at the LHC.

D. A look at experimental data

The left panel of Fig. 7 shows the famous experimental plot by Voloshin [21] which provides empirical evidence for multiplicity scaling of v_2/ε . The lines labelled “HYDRO” are sketches for expectations from ideal fluid dynamics, based on the calculations presented in [25] for v_2 in Au+Au collisions at fixed impact parameter $b = 7$ fm as a function of multiplicity (parametrized by e_0). They should be replaced by the curves shown in the left panels of Fig. 5.

In the middle and right panel we present multiplicity scaling curves for v_2/ε obtained from viscous hydrodynamics with the full I-S equations (middle panel) and in the simplified I-S approach (right panel). The comparison shows that using the simplified I-S approach can be quite misleading since, especially for larger than minimal values of η/s , the simplified approach significantly overpredicts the viscous suppression of elliptic flow unless one first extrapolates it to the Navier-Stokes point $\tau_\pi = 0$ (this was not done in Fig. 7). The middle panel shows results from the less τ_π -sensitive and thus more reliable full I-S approach. On a superficial level, the theoretical curves show qualitative similarity with the experimental data, giving correct ball-park numbers if one assumes $\eta/s \sim 0.24 \sim 3/4\pi$. Interestingly, ignoring experimental error bars, one can see evidence for small scaling viola-

tions in the experimental data whose pattern agrees with the theoretical predictions from viscous hydrodynamics (see discussion at the end of Sec. V A): the 62.5 A GeV Au+Au data lie slightly above the 200 A GeV Au+Au points, and the 200 A GeV Cu+Cu points fall slightly below the 62.5 A GeV Au+Au data. Of course, these fine features of the experimental data are presently not statistically significant; much more precise data are needed to confirm or disprove the theoretical predictions, but upcoming high-statistic runs at RHIC should be able to deliver them.

Closer inspection of the two left panels in Fig. 7 shows, however, that the theoretical scaling curves have the wrong slope: on the left side of the plot, i.e. for small multiplicity densities, the data seem to point towards larger specific shear viscosities $\frac{\eta}{s} > 3 \times \frac{1}{4\pi}$ whereas on the right side of the plot, for $\frac{1}{S} \frac{dN_{\text{ch}}}{dy} > 20 \text{ fm}^{-2}$, the experimental data require smaller shear viscosities, $\frac{\eta}{s} \lesssim (1-2) \times \frac{1}{4\pi}$. But this is not at all unexpected: Collisions represented by points in the right half of the plot correspond to high collision energies and large initial energy densities whose expanding fireballs spend the largest fraction of their life in the QGP phase. Fireballs created in collisions represented by points in the left part of the diagram have smaller initial energy densities and thus spend most of their time in the much more viscous hadronic phase [19]. A meaningful comparison between theory and experiment thus must necessarily account for the temperature dependence of η/s and its dramatic increase during the quark-hadron phase transition [50]. This would lead to scaling curves in Fig. 7b with a larger slope that can better reproduce the data. What one can say already now is that the high-energy end of Fig. 7 requires very small specific shear viscosity η/s for the QGP, of the same order as the minimal value postulated in [16, 17] (unless the initial source eccentricity ε was strongly underestimated in the experimental data).

VI. MULTIPLICITY SCALING OF ENTROPY PRODUCTION IN VISCOUS HYDRODYNAMICS

In the absence of shock waves, ideal fluid dynamics conserves entropy. Correspondingly, the final multiplicity per unit rapidity is directly determined by total initial entropy per unit rapidity: $\frac{dN}{dy} = \text{const.} \times \tau_0 \int dx dy s(x, y; \tau_0)$. The flux-corrected transport algorithm SHASTA used in the numerical solution of both the ideal and viscous fluid equations [3, 47] employs an antidiffusion step to dampen unwanted numerical oscillations near shock waves that can arise from first order phase transitions. This step induces a small amount of “numerical viscosity” which can not be fully avoided. In all our simulations we used 0.125 for the antidiffusion constant [57], resulting in about 0.3% entropy production by numerical viscosity in the ideal fluid case. In comparison with the $\mathcal{O}(10-15\%)$ entropy production in a viscous fluid with minimal shear viscosity (see below)

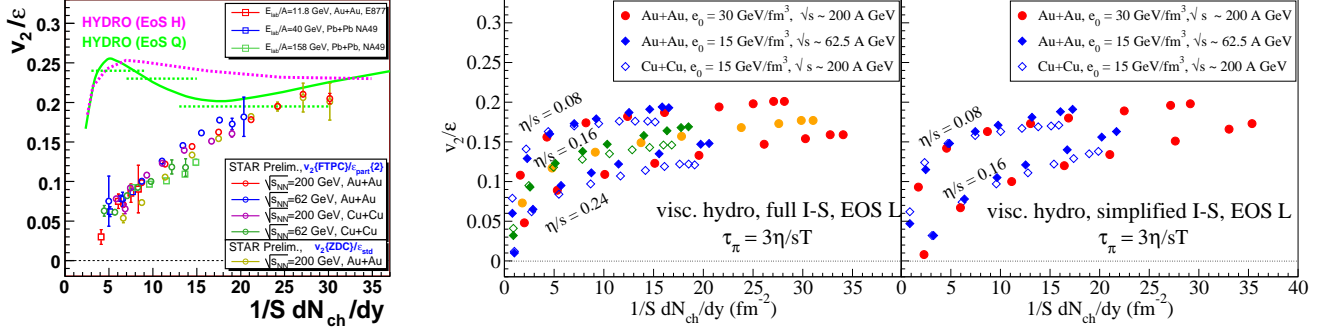


FIG. 7: (Color online) Left: The experimental observation of multiplicity scaling for v_2/ϵ , with data from Au+Au, Pb+Pb, and Cu+Cu collisions at RHIC, SPS and AGS [21]. Middle: Theoretical prediction of approximate multiplicity scaling from viscous hydrodynamics using the full I-S equations, for three different (constant) specific entropy values $\eta/s = 0.08, 0.16, 0.24$. Right: Same as middle panel, but using the simplified I-S equations for $\eta/s = 0.08$ and 0.16 .

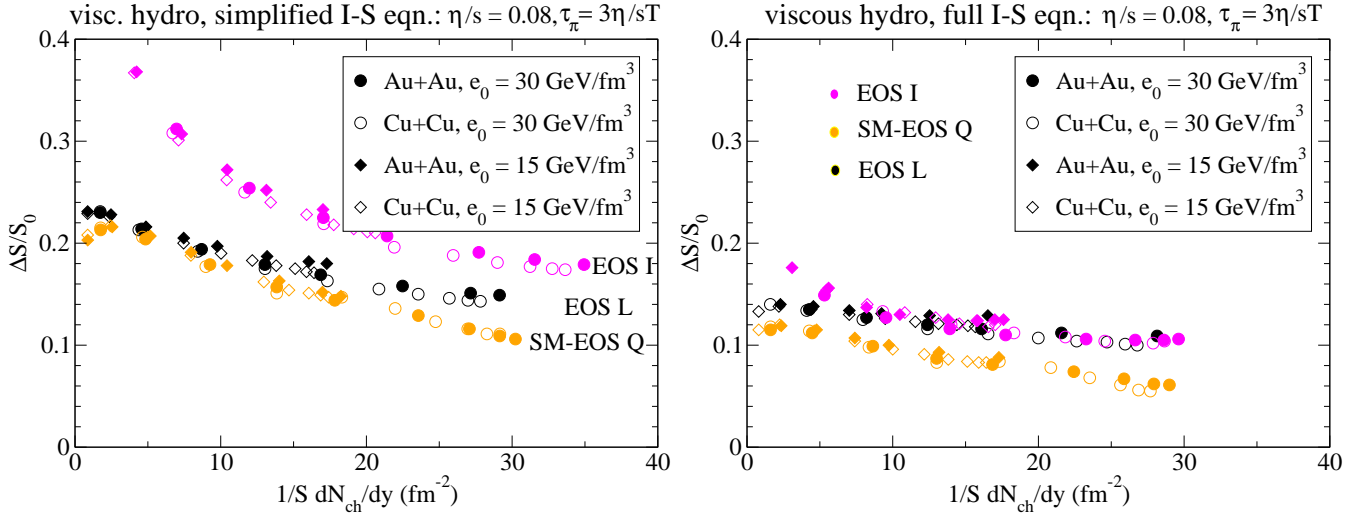


FIG. 8: (Color online) Entropy production ΔS , normalized by the initial entropy S_0 , as a function of charged multiplicity density $\frac{1}{S} \frac{dN_{ch}}{dy}$. Calculations with VISH2+1 were performed for Au+Au and Cu+Cu collisions at various impact parameters and collision energies, using $\eta/s = 0.08$, $\tau_\pi = 3\eta/sT$, and three different equations of state (EOS I, SM-EOS Q, and EOS L). Left panel: Simplified I-S equations. Right panel: Full I-S equations.

this can be neglected.

Similar to the second paper of Ref. [46], we compute entropy production by exploiting the proportionality of final entropy to final charged multiplicity. We compute the final multiplicity dN_{ch}/dy for both ideal and viscous hydrodynamics and then equate the fractional increase in dN_{ch}/dy with the fractional increase in dS/dy . This ignores a small negative correction due to the viscous deviation of the distribution function on the freeze-out hypersurface from local equilibrium [38, 41] which slightly reduces the entropy per finally observed particle in the viscous case. Since on the freeze-out surface the viscous pressure components are small [3], this correction should be negligible. We do note, however, that our viscous evolution starts earlier (at $\tau_0 = 0.6 \text{ fm}/c$) than that of Ref. [46] (who use $\tau_0 = 1 \text{ fm}/c$), which results in larger entropy production fractions. We confirmed that the dif-

ference is quantitatively reproduced by the entropy generated during the time interval between 0.6 and $1.0 \text{ fm}/c$, which can be calculated to good approximation analytically [18] (using Eq. (D3) in Ref. [3]) by assuming boost-invariant longitudinal expansion without transverse flow during this period.

Figure 8 shows the viscous entropy production ΔS , as a fraction of the initial entropy S_0 , for Cu+Cu and Au+Au collisions at various impact parameters and collision energies, as a function of multiplicity density. One observes approximate multiplicity scaling of the fractional entropy production, with scaling functions that depend on the equation of state and, for non-zero kinetic relaxation time, on the form of the Israel-Stewart equations used in the simulation. As with v_2/ϵ we see small scale-breaking effects, but generally the produced entropy fraction shows better multiplicity scaling than

elliptic flow. The scale breaking effects for the viscous entropy production rate go in the same direction as with elliptic flow insofar as, at the same value of $\frac{1}{S} \frac{dN_{ch}}{dy}$, larger collision systems and more central collisions produce fractionally more entropy than smaller or more peripheral collisions, due to their longer lifetimes before freeze-out.

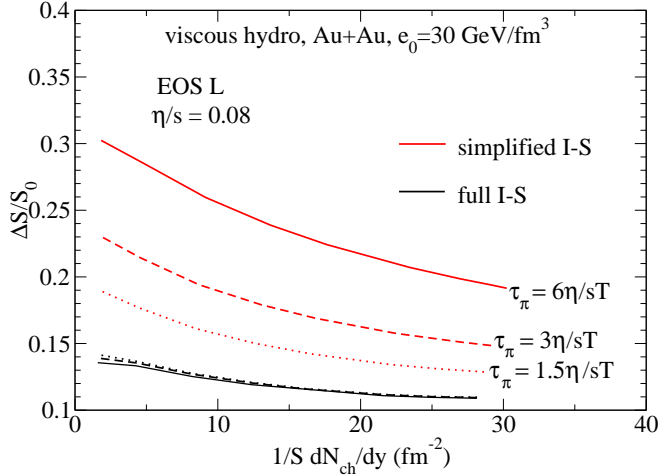


FIG. 9: (Color online) Sensitivity of the entropy production ratio $\Delta S/S_0$ shown in Fig. 8 to the kinetic relaxation time τ_π , for the Au+Au collision system with $e_0 = 30 \text{ GeV/fm}^3$ (corresponding to a collision energy of $\sqrt{s} \approx 200 \text{ A GeV}$). The three red curves (upper set) are for the simplified Israel-Stewart equations, the three black curves (lower set) for the full I-S equations. Solutions with the full I-S equations produce less entropy and show very little sensitivity to τ_π .

For $\tau_\pi = 3\eta/sT$, Figure 8 shows that the simplified I-S equations (left panel) result in almost twice as much entropy production as the full I-S system! Figure 9 clarifies that, when the simplified I-S equations are used, entropy production depends very sensitively on the kinetic relaxation time τ_π , approaching the much smaller and almost completely τ_π -independent entropy production rates of the full I-S framework in the limit $\tau_\pi \rightarrow 0$. The large amount of extra entropy production for non-zero τ_π in the simplified I-S approach must thus be considered as unphysical. This is important because this artificial extra entropy production (caused by unphysically large excursions of the viscous shear pressure tensor π^{mn} away from its Navier-Stokes value $\pi^{mn} = 2\eta\sigma^{mn}$) manifests itself as additional charged hadron multiplicity in the observed final state (seen as a shift of all points in the left panel of Fig. 8 towards larger values of $\frac{1}{S} \frac{dN_{ch}}{dy}$). Since the final multiplicity is used to normalize the initial energy density e_0 , this causes a significant distortion of the initial conditions corresponding to a given set of experimental data, affecting their physical interpretation.

We conclude that using the full I-S equations is mandatory if one wants to minimize artificial effects of shear viscosity on entropy production and elliptic flow in the realistic situation of non-zero kinetic relaxation times. (We note that, while the value of τ_π for the QGP created

at RHIC is presently unknown, it can obviously not be zero.) From the right panel in Fig. 8 we see that this removes most of the large difference in entropy production between the rapidly exploding EOS I fireballs and their more leisurely expanding cousins that evolve under the influence of EOS Q or EOS L. Still, even for the full I-S equations we see 15–25% differences between the entropy production rates for EOS Q (first order phase transition) and EOS L (rapid crossover transition). The differences are largest for the most central Au+Au and Cu+Cu collisions at top RHIC energies. The somewhat stiffer nature of EOS L near T_c causes the fireball to expand faster and with higher acceleration, leading to larger viscous effects than for EOS Q. The differences in entropy production caused by this variation of the EOS is of similar magnitude as its effect on the viscous suppression of v_2/ε discussed at the end of Sec. IV.

An important comment relates to the negative overall slope of the scaling curves for entropy production shown in Figs. 8 and 9: Since peripheral collisions produce relatively more entropy than central collisions, and the produced entropy is reflected in the final charged hadron multiplicity, the collision centrality dependence of hadron multiplicities is altered by viscous effects. When viscous effects are accounted for, the charged multiplicity dN_{ch}/dy will rise more slowly as a function of the number of participant nucleons N_{part} than for an ideal fluid with the same set of initial conditions. In a Glauber model parametrization of the initial conditions [8] this tempering effect will have to be compensated for by increasing the “hard” component in the initial entropy production, i.e. the component that scales with the density of binary collisions and is thus responsible for the non-linear increase of dN_{ch}/dy with N_{part} . In the color glass condensate approach [58] this non-linear rise is controlled by the centrality dependence of the saturation momentum scale Q_s , with no free parameters to tune. It remains to be seen whether the success of the CGC model in describing the centrality dependence of dN_{ch}/dy [59] survives the inclusion of entropy (or multiplicity) producing effects resulting from shear viscosity during the evolution from the initial CGC to the finally observed state.

VII. CONCLUDING REMARKS

The main motivation for the work presented in this paper was provided by the experimentally observed multiplicity scaling of the elliptic flow, shown in Fig. 7a, and its deviation at low multiplicities from ideal fluid dynamical predictions. We saw that many of the observed features are qualitatively consistent with viscous hydrodynamic calculations as presented in this paper, and that the same calculations also predict approximate multiplicity scaling for viscous entropy production. Our studies revealed, however, that even for ideal fluid dynamics the multiplicity scaling of the elliptic flow is not perfect, with small scaling violations introduced by the freeze-out pro-

cess which cuts the evolution of elliptic flow short. Even at RHIC energies, where the elliptic flow almost saturates before freeze-out, kinetic decoupling truncates the momentum anisotropy at values slightly below their asymptotic saturation value, and the deviations depend on the size of the colliding nuclei and the deformation of the fireball created in the collision through the time available for building elliptic flow before freeze-out.

Shear viscosity strongly suppresses the build-up of momentum anisotropy and elliptic flow, especially for low multiplicity densities, i.e. at large impact parameters, low collision energies or for small sizes of the colliding nuclei. This changes the slope of the multiplicity scaling curve for v_2/ε but preserves, to good approximation, its general scaling with $\frac{1}{S} \frac{dN_{ch}}{dy}$. Violations of multiplicity scaling for v_2/ε are somewhat larger for the viscous expansion than for the ideal fluid (especially with EOS I), but remain small enough to be consistent, within statistical errors, with the experimental observation of approximate scaling. The slope of the approximate scaling curve and the spread around this curve caused by scaling violation increase with the value of the specific shear viscosity η/s and can thus be used to constrain it.

Specifically, the observed scaling violations have the following features: At fixed multiplicity density $\frac{1}{S} \frac{dN_{ch}}{dy}$, viscous hydrodynamics predicts slightly larger elliptic flow v_2/ε for larger collision systems or more central collisions than for smaller nuclei colliding at similar energy or more peripheral collisions between similar-size nuclei colliding at higher energy. Larger v_2/ε values are associated with longer lifetimes of the corresponding fireballs before freeze-out and thus also with larger relative entropy production. This correlates the scaling violations for v_2/ε observed in Figs. 5 and 7 with those for the relative entropy production $\Delta S/S_0$ seen in Fig. 8. The pattern of the predicted scaling violations shows qualitative agreement with experiment, although higher quality data are required to render this agreement statistically robust and quantitative.

For a fixed (i.e. temperature independent) ratio η/s , the slope of the multiplicity scaling curve for v_2/ε does not agree with experiment – the curves predicted by viscous hydrodynamics are too flat. The slope can be increased by allowing η/s to increase at lower temperatures: For small multiplicity densities (very peripheral collisions or low collision energies), the data seem to require $\frac{\eta}{s} > 3 \times \frac{1}{4\pi}$, whereas at large multiplicity densities they appear to constrain the specific shear viscosity to values of $\frac{\eta}{s} \lesssim (1-2) \times \frac{1}{4\pi}$. While this is qualitatively consistent with the idea that in high-multiplicity events the dynamics is dominated by the QGP phase (whose viscosity would thus have to be small, of order $1/4\pi$) whereas low-multiplicity events are predominantly controlled by hadron gas dynamics (which is highly viscous [19]), much additional work is needed to turn this observation into quantitative constraints for the function $\frac{\eta}{s}(T)$.

The present study also resolves questions that arose

from several recent publications of viscous hydrodynamic calculations which seemed to yield different results. We explored the effects of using different implementations of Israel-Stewart second order theory for causal relativistic viscous hydrodynamics, by comparing the “simplified Israel-Stewart equations” previously used by us [3] with the “full Israel-Stewart equations” implemented by P. & U. Romatschke [1]. For the “simplified” approach we found a strong sensitivity of physical observables on the presently unknown kinetic relaxation time τ_π for the viscous shear pressure tensor π^{mn} , in contrast to a much weaker and basically negligible τ_π -dependence in the “full” approach. For non-zero τ_π the “simplified I-S equations” allow for large excursions of π^{mn} away from its Navier-Stokes limit $\pi^{mn} = 2\eta\sigma^{mn}$. These excursions are artificial and disappear in the Navier-Stokes limit $\tau_\pi \rightarrow 0$ which can, however, not be stably simulated numerically. They cause large viscous suppression effects for the elliptic flow and large amounts of extra entropy production (i.e. extra final hadron multiplicity). From our study we conclude that the “simplified I-S approach” should be avoided, and that a reliable extraction of η/s from experimental data mandates the use of the “full Israel-Stewart equations” [1, 52]. (It is, however, permissible to use the conformal fluid approximation [1, 34] for the “full I-S equations” even if the fluid’s EOS is not conformally invariant since the differences were found to be negligible.)

In comparing our previous work [3] with that of others we also identified other factors that significantly influence the creation of elliptic flow and thus help to account for the observed differences. For a realistic equation of state that implements a quark-hadron transition (here SM-EOS Q and EOS L), it turns out that a much more important effect than using the correct version of Israel-Stewart theory is the size of the colliding nuclei. At RHIC energies and for a realistic EOS, the viscous suppression effects for v_2/ε in Cu+Cu collisions are almost twice as large as for the larger Au+Au collision system. Non-negligible differences in the amount of viscous v_2 suppression arise also from details in the EOS, with a smooth crossover as implemented in EOS L giving 25-30% less suppression than a first-order transition as in SM-EOS Q. Compared to system size effects and EOS uncertainties, the differences between “simplified” and “full” I-S theory are relatively small, affecting the viscous v_2 suppression at the 10% level relative to each other. (The quoted percentages are for a fluid with minimal viscosity $\eta/s = 1/4\pi$ and may be larger for higher viscosity.) The largest uncertainty, in any case, is contributed by our present lack of knowledge of the initial source eccentricity which contributes a theoretical error band of up to 30% on an absolute scale for v_2 [19, 52–54].

We finally comment that the multiplicity dependence of viscous entropy production predicted by viscous hydrodynamics (see Fig. 8) will modify the centrality dependence of charged hadron production. This issue will be studied more quantitatively in a forthcoming paper.

Acknowledgments

We thank K. Dusling, P. Huovinen, M. Lisa, P. Romatschke, and D. Teaney for fruitful discussions and use-

ful comments on the manuscript. This work was supported by the U.S. Department of Energy under contract DE-FG02-01ER41190.

-
- [1] P. Romatschke and U. Romatschke, Phys. Rev. Lett. **99**, 172301 (2007).
 - [2] A. K. Chaudhuri, arXiv:0704.0134 [nucl-th]; arXiv:0708.1252 [nucl-th]; arXiv:0801.3180 [nucl-th]; and arXiv:0803.0643 [nucl-th].
 - [3] H. Song and U. Heinz, Phys. Lett. B **658**, 279 (2008); and Phys. Rev. C, in press [arXiv:0712.3715 [nucl-th]].
 - [4] K. Dusling and D. Teaney, Phys. Rev. C **77**, 034905 (2008).
 - [5] U. Heinz and S. M. H. Wong, Phys. Rev. C **66**, 014907 (2002).
 - [6] D. Teaney, Phys. Rev. C **68**, 034913 (2003).
 - [7] The experimental situation is summarized in I. Arsene *et al.* [BRAHMS Collaboration] Nucl. Phys. A **757**, 1 (2005); B.B. Back *et al.* [PHOBOS Collaboration], Nucl. Phys. A **757**, 28 (2005); J. Adams *et al.* [STAR Collaboration], Nucl. Phys. A **757**, 102 (2005); K. Adcox *et al.* [PHENIX Collaboration], Nucl. Phys. A **757**, 184 (2005).
 - [8] Recent theoretical reviews include: P. Huovinen, in *Quark Gluon Plasma 3*, edited by R. C. Hwa and X. N. Wang (World Scientific, Singapore, 2004), p. 600 [nucl-th/0305064]; P. F. Kolb and U. Heinz, *ibid.*, p. 634 [nucl-th/0305084]; P. Huovinen and P. V. Ruuskanen, Ann. Rev. Nucl. Part. Sci. **56**, 163 (2006).
 - [9] U. Heinz, J. Phys. G: Nucl. Part. Phys. **31**, S717 (2005);
 - [10] R. A. Lacey *et al.*, Phys. Rev. Lett. **98**, 092301 (2007).
 - [11] U. Heinz and P. F. Kolb Nucl. Phys. A **702**, 269 (2002).
 - [12] U. Heinz, AIP Conf. Proc. **739**, 163 (2005) [arXiv:nucl-th/0407067].
 - [13] M. Gyulassy, in *Structure and dynamics of elementary matter*, edited by W. Greiner *et al.*, NATO Science Series II: Mathematics, Physics and Chemistry, Vol. **166** (Kluwer Academic, Dordrecht, 2004), p. 159-182 [arXiv:nucl-th/0403032].
 - [14] M. Gyulassy and L. McLerran, Nucl. Phys. A **750**, 30 (2005).
 - [15] E. V. Shuryak, Nucl. Phys. A **750**, 64 (2005).
 - [16] G. Policastro, D. T. Son and A. O. Starinets, Phys. Rev. Lett. **87**, 081601 (2001); JHEP **0209**, 043 (2002).
 - [17] P. Kovtun, D. T. Son and A. O. Starinets, Phys. Rev. Lett. **94**, 111601 (2005).
 - [18] P. Danielewicz and M. Gyulassy, Phys. Rev. D **31**, 53 (1985).
 - [19] T. Hirano, U. Heinz, D. Kharzeev, R. Lacey and Y. Nara, Phys. Lett. B **636**, 299 (2006); J. Phys. G **34**, S879 (2007); and Phys. Rev. C, in press [arXiv:0710.5795 [nucl-th]].
 - [20] C. Alt *et al.* [NA49 Collaboration], Phys. Rev. C **68**, 034903 (2003);
 - [21] S. A. Voloshin, J. Phys. G **34**, S883 (2007); and AIP Conf. Proc. **870**, 691 (2006) [arXiv:nucl-ex/0610038].
 - [22] R. C. Hwa and K. Kajantie, Phys. Rev. D **32**, 1109 (1985).
 - [23] J. Y. Ollitrault, Phys. Rev. D **46**, 229 (1992).
 - [24] R. S. Bhalerao, J. P. Blaizot, N. Borghini and J. Y. Ollitrault, Phys. Lett. B **627**, 49 (2005).
 - [25] P. F. Kolb, J. Sollfrank and U. Heinz, Phys. Lett. B **459**, 667 (1999); and Phys. Rev. C **62**, 054909 (2000).
 - [26] H. Heiselberg and A. M. Levy, Phys. Rev. C **59**, 2716 (1999);
 - [27] S. A. Voloshin and A. M. Poskanzer, Phys. Lett. B **474**, 27 (2000);
 - [28] H. J. Drescher, A. Dumitru, C. Gombeaud and J. Y. Ollitrault, Phys. Rev. C **76**, 024905 (2007) [arXiv:0704.3553 [nucl-th]].
 - [29] K. Paech and S. Pratt, Phys. Rev. C **74**, 014901 (2006).
 - [30] D. Kharzeev and K. Tuchin, arXiv:0705.4280 [hep-ph].
 - [31] H. B. Meyer, arXiv:0710.3717 [hep-lat].
 - [32] U. Heinz, H. Song and A. K. Chaudhuri, Phys. Rev. C **73**, 034904 (2006).
 - [33] A. Muronga and D. H. Rischke, arXiv:nucl-th/0407114.
 - [34] R. Baier, P. Romatschke, D. T. Son, A. O. Starinets and M. A. Stephanov, arXiv:0712.2451 [hep-th].
 - [35] S. Bhattacharyya, V. E. Hubeny, S. Minwalla and M. Rangamani, JHEP **0802**, 045 (2008).
 - [36] M. Natsuume and T. Okamura, Phys. Rev. D **77**, 066014 (2008); and M. Natsuume and T. Okamura, arXiv:0801.1797 [hep-th].
 - [37] R. Loganayagam, arXiv:0801.3701 [hep-th].
 - [38] W. Israel, Ann. Phys. (NY) **100** (1976) 310; W. Israel and J. M. Stewart, Phys. Lett. **58A**, 213 (1976); W. Israel and J. M. Stewart, Ann. Phys. (NY) **118** (1979) 341.
 - [39] A. Muronga, Phys. Rev. Lett. **88**, 062302 (2002) [Erratum: *ibid.* **89**, 159901 (2002)];
 - [40] A. Muronga, Phys. Rev. C **69**, 034903 (2004);
 - [41] A. Muronga, Phys. Rev. C **76**, 014909 and 014910 (2007).
 - [42] R. Baier, P. Romatschke and U. A. Wiedemann, Phys. Rev. C **73**, 064903 (2006).
 - [43] I. Müller, Z. Phys. **198**, 329 (1967).
 - [44] M. Grmela, H. C. Öttinger, Phys. Rev. E **56**, 6620 (1997); H. C. Öttinger, M. Grmela, Phys. Rev. E **56**, 6633 (1997); H. C. Öttinger, Phys. Rev. E **57**, 1416 (1998).
 - [45] A. K. Chaudhuri and U. Heinz, J. Phys.: Conf. Ser. **50**, 251 (2006);
 - [46] R. Baier and P. Romatschke, Eur. Phys. J. C **51**, 677 (2007); P. Romatschke, Eur. Phys. J. C **52**, 203 (2007).
 - [47] The (2+1)-d ideal fluid code AZHYDRO can be downloaded from URL <http://nt3.phys.columbia.edu/people/molnard/OSCAR/>.
 - [48] F. Cooper and G. Frye, Phys. Rev. D **10**, 186 (1974).
 - [49] S.D. Katz, Nucl. Phys. A **774**, 159 (2006).
 - [50] T. Hirano and M. Gyulassy, Nucl. Phys. A **769**, 71 (2006).
 - [51] P. Huovinen, Nucl. Phys. A **761**, 296 (2005).
 - [52] M. Luzum and P. Romatschke, arXiv:0804.4015 [nucl-th].
 - [53] A. Adil, H. J. Drescher, A. Dumitru, A. Hayashigaki and Y. Nara, Phys. Rev. C **74**, 044905 (2006); H. J. Drescher and Y. Nara, Phys. Rev. C **75**, 034905 (2007).

- [54] T. Lappi and R. Venugopalan, Phys. Rev. C **74**, 054905 (2006).
- [55] Y. Aoki, Z. Fodor, S. D. Katz and K. K. Szabo, Phys. Lett. B **643**, 46 (2006).
- [56] M. Cheng *et al.*, Phys. Rev. D **74**, 054507 (2006).
- [57] H. Von Gersdorff, L. D. McLerran, M. Kataja and P. V. Ruuskanen, Phys. Rev. D **34**, 794 (1986).
- [58] D. Kharzeev and M. Nardi, Phys. Lett. B **507**, 121 (2001); D. Kharzeev, E. Levin and M. Nardi, Phys. Rev. C **71**, 054903 (2005).
- [59] D. Kharzeev and E. Levin, Phys. Lett. B **523**, 79 (2001).